TU Delft

Delft University of Technology

Buckling of 3D-Printed Cylindrical Shells with Corrugated Surface

Labans, Edgars; Bisagni, Chiara

DOI
10.2514/6.2020-1925

Publication date
2020

Document Version
Final published version

Published in
AIAA Scitech 2020 Forum

Citation (APA)
Labans, E., & Bisagni, C. (2020). Buckling of 3D-Printed Cylindrical Shells with Corrugated Surface. In *AIAA Scitech 2020 Forum: 6-10 January 2020, Orlando, FL* Article AIAA 2020-1925 (AIAA Scitech 2020 Forum; Vol. 1 PartF). American Institute of Aeronautics and Astronautics Inc. (AIAA). https://doi.org/10.2514/6.2020-1925

Important note
To cite this publication, please use the final published version (if applicable).
Please check the document version above.

Copyright
Other than for strictly personal use, it is not permitted to download, forward or distribute the text or part of it, without the consent of the author(s) and/or copyright holder(s), unless the work is under an open content license such as Creative Commons.

Takedown policy
Please contact us and provide details if you believe this document breaches copyrights.
We will remove access to the work immediately and investigate your claim.

This work is downloaded from Delft University of Technology.
For technical reasons the number of authors shown on this cover page is limited to a maximum of 10.

AIAA SciTech Forum
6-10 January 2020, Orlando, FL
AIAA Scitech 2020 Forum

10.2514/6.2020-1925

Check for updates

Buckling of 3D-Printed Cylindrical Shells with Corrugated Surface

Edgars Labans[1] and Chiara Bisagni[2]
Delft University of Technology, Delft, 2629HS, Netherlands

3D-printing technology opens broad possibilities to manufacture structural shapes which could not be always possible by other methods. In the field of lightweight shells it allows to investigate structures with higher buckling loads than conventional shells. The buckling behavior of 3D-printed shells is studied in this paper where the shape of the cylindrical shells is modified by adding corrugation in the axial or circumferential directions. The shells are characterized by the amplitude of the corrugation and the number of the sinusoidal waves. Their elastic mechanical behavior is analyzed up to the buckling load. The numerical analysis shows that the modified surface can significantly improve the buckling load and reduces the sensitivity towards geometric imperfections. Prototypes of the shells were manufactured and tested to validate the numerical model. Regardless the experimental scatter, the average buckling load of the optimized corrugated shell twice exceeds the buckling load of the reference circular shell. At the same time stiffness and mass of the shell remain the same.

Downloaded by TU DELFT on January 7, 2020 | http://arc.aiaa.org | DOI: 10.2514/6.2020-1925

I. Nomenclature

A_m, A_n	=	Axial and circumferential corrugation amplitude
a_m, a_n	=	Axial and circumferential corrugation amplitude/radius ratio
DIC	=	Digital image correlation
h	=	Height of the shell
m	=	Number of sinusoidal waves along the height of the shell
MDF	=	Medium Density Fiberboard
n	=	Number of sinusoidal waves along the circumference of the shell
PLA	=	Polylactide
r_0	=	Nominal radius of the shell
t	=	Thickness of the shell

II. Introduction

Cylindrical shells are one of the most common structures in aircraft fuselages and space launch vehicles. Because of the exceptional load bearing capacity of curved shells, their thickness can be very thin, and consequently it leads to the situation where buckling is one of the main design cases. Existing research extensively explores the stability of shells made of conventional materials like carbon fiber reinforced plastics[1–4] or metallic sheets[5,6], however, thin-walled structures made by additive manufacturing received only minor attention. Although 3D-printing could provide substantial advantage, allowing broader geometric variations and also the possibility to change the thickness of the shell locally.

The research on large scale 3D-printed shells is not yet fully considered mainly because of the manufacturing limitations on large scale. More often shells made by additive manufacturing appears in literature as the bio-mimicking of natural structures[7], folded origami parts with shape memory[8] or the prototyping of small-scale aircraft components[9].

The possibility to manufacture 3D-printed cylindrical shells with modified geometry can increase the buckling load and reduce the sensitivity to geometric imperfections. Recent numerical research was conducted by Sowiński[10] on barreled, pseudo-barreled and cylindrical shells. It was demonstrated that surface corrugation could increase load-bearing capacity of all three investigated shell shapes, and in some cases even reduce the impact of the imperfections.

[1] Post-doctoral Researcher, Faculty of Aerospace Engineering.
[2] Professor, Faculty of Aerospace Engineering, AIAA Associate Fellow.

Copyright © 2020 by the American Institute of Aeronautics and Astronautics, Inc. All rights reserved.

Ning and Pellegrino[11,12] performed numerical and also experimental work on waved composite cylindrical shells with the aim to design shells that are insensitive towards geometric imperfections. Previous research efforts to reduce the imperfection sensitivity of the shells were mainly focused on integrating vertical or horizontal stiffeners[13], applying variable angle-tow composites[14,15] or optimized laminate stacking[16].

This study is focused on the numerical and experimental investigation of the buckling behavior of 3D-printed cylindrical shells with corrugated surface, which can provide higher buckling load and less sensitivity towards initial geometric imperfections than conventional cylindrical shells. Although corrugated surface could be also manufactured by using conventional stamping press, this shape is chosen as a starting point of introducing additive manufacturing in the thin-walled shell design. Further, it can be upgraded to more sophisticated configurations. The tests on small specimens can help to understand the influence of different corrugated shapes before proceeding to large structures.

The research is divided in consecutive steps: 1) building the numerical models of the shells with different corrugation types; 2) manufacturing and performing axial compression tests of the shells; 3) optimizing the corrugation parameters to reach highest buckling load; 4) performing experimental tests on the optimized shells.

III. Shells with Corrugated Surface

At first, shells with regular cylindrical shapes are analyzed. Then, the shell geometry is modified by introducing surface corrugation along the height and around the circumferential direction as shown in Fig. 1.

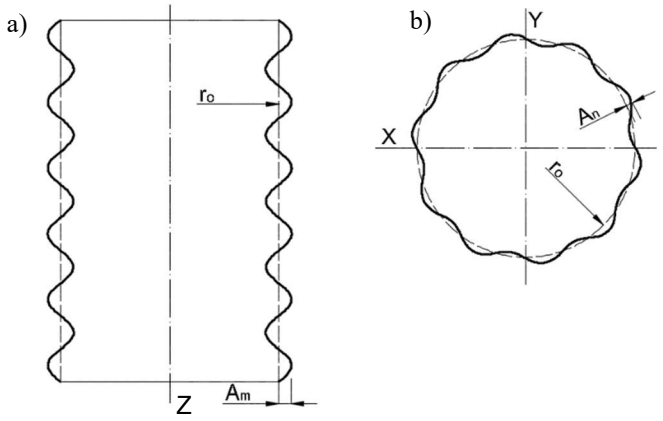

Fig. 1 Geometric parameters of the corrugation: a) side view of axially corrugated shell; b) top view of circumferentially corrugated shell.

The corrugation is defined by sinusoidal wave functions. The amplitude of the corrugation waves along the height of the shell is marked with A_m and around circumference with A_n. The amplitude of the corrugation is tied to the nominal radius of the cylindrical shell as given in equation (1):

$$a_m = \frac{A_m}{r_0}; \qquad a_n = \frac{A_n}{r_0} \tag{1}$$

In this study the dimensions of the shells is limited by the available 3D-printing devices, thus the height is assumed equal to 170 mm. Two sets of the shell radius are used: 50 mm and 75 mm. The minimal thickness of the shell achievable with conventional filament based 3D printers is 0.2 mm and the printer nozzle diameter step is 0.1 mm. The shells are made of polylactide (PLA) filament with modulus of elasticity equal to 2.34 GPa and density equal to 1240 kg/m^3. The plastic yield stress for PLA filament is 46 MPa[17]. Medium Density Fiberboard (MDF) with the thickness of 6 mm is used as the inner end-rings of the shells. The mechanical properties of the MDF are taken from literature[18].

Downloaded by TU DELFT on January 7, 2020 | http://arc.aiaa.org | DOI: 10.2514/6.2020-1925

IV. Numerical Analysis

Numerical finite element (FE) analyses are performed using ABAQUS 2019, and the input files for the FE analysis are prepared in MATLAB environment. General purpose, reduced integration S4R shell elements with mesh size of 2 mm are chosen by performing a mesh sensitivity study. Examples of the FE meshes are shown in Fig. 2 for axially and circumferentially corrugated shells.

The first set of shells analyzed here have radius equal to 50 mm and height equal to 170 mm. The boundary conditions restrict all the translations and rotations on the nodes at the bottom-end of the shells, while the nodes on the upper-end have similar boundary conditions, except that translation along vertical axis is allowed. The upper nodes are also connected together with kinematic coupling, which allows applying load at a single reference node.

Two types of analyses are performed: linear eigenvalue analysis to evaluate the buckling load, and non-linear static analysis to assess the influence of the initial geometric imperfections on the buckling load. It should be noted that the corrugated surface of the shells is not considered as initial geometric imperfections. The source of the initial geometric imperfections in the non-linear analysis is the first eigenmode of the linear buckling analysis. The amplitude of the imperfection is tied to the value of the wall thickness and is usually in the range of 10% of the wall thickness.

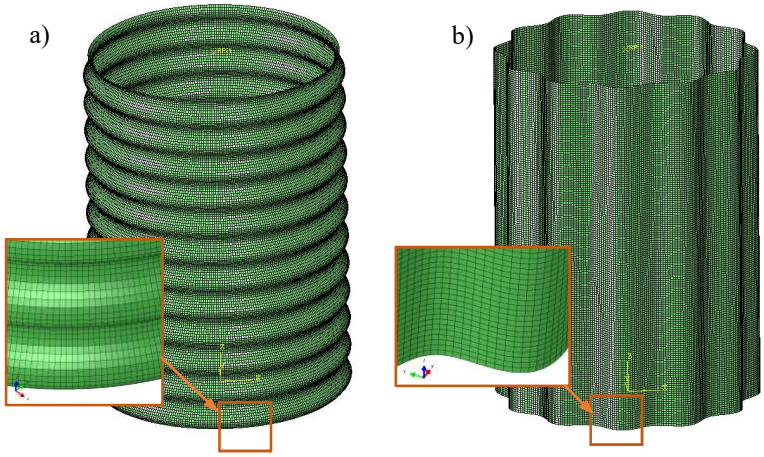

Fig. 2 FE meshes: a) axially corrugated shell; b) circumferentially corrugated shell.

V. Preliminary Tests

For the tests, three variations of the 3D-printed shells, circular shells, axially corrugated shells and circumferentially shells, are manufactured for the preliminary tests using commercially available Creality Ender 3D printer and PLA filament. Three shells of each variation are made.

The circular shells without corrugation, shown in Fig. 3a, serve as reference to assess relative performance of the shells with axial and circumferential corrugation shown in Fig. 3b and Fig. 3c, respectively.

The corrugation parameters for this first set of shells are chosen considering the optimal values for the steel shells with the radius/thickness ratio in the range of 160-190 reported in the work of Sowiński[10]. The manufactured shells have a wall thickness equal to 0.4 mm, so the radius/thickness ratio is 125. For the shells with corrugation along the height 12 corrugation waves are used, with $a_m = 0.05$. The shells with corrugation along the circumference have 15 waves with $a_n = 0.05$.

As optimization is not considered in this step, all shells have the same wall thickness formed in the result of printing in spiralizer contour mode. All shells are equipped with end reinforcement rings made of 6 mm thick MDF. The width of the potting is 8 mm and it is bonded to the shell from inside by polyvinyl acetate adhesive.

Downloaded by TU DELFT on January 7, 2020 | http://arc.aiaa.org | DOI: 10.2514/6.2020-1925

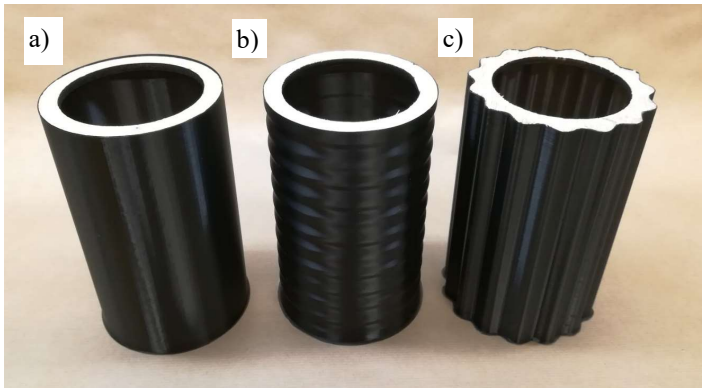

Fig. 3 Shell prototypes: a) reference shell; b) axially corrugated shell; c) circumferentially corrugated shell.

The compression tests are performed on Zwick Z20 mechanical test machine with 20 kN load capacity. The shells are located between two parallel steel plates and compressed in displacement controlled test with the loading rate of 0.5 mm/min. The test set-up is shown in Fig. 4. A Digital Image Correlation (DIC) system is used to capture the axial displacement of the shell and also the out-of-plane displacements of the buckling shape. The shells are painted with contrasting dotted pattern to allow better surface tracking by DIC system.

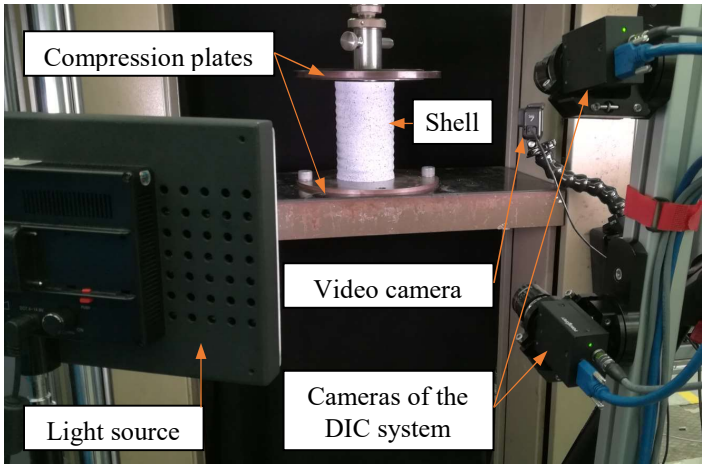

Fig. 4 Test set-up.

The experimental load-shortening curves together with the images of the post-buckling shapes are displayed in Fig. 5. In general, good repeatability of the stiffness is observed for all three shells. The average buckling load of the reference shells shown in Fig. 5a is 791 N with standard deviation of 36 N. One of the possible explanation of this scatter might be high sensitivity to the imperfections of the boundary conditions. As the reinforcement rings are glued to the shells manually, the bond line might contain weaker spots or gaps invisible from outside. Additional outer reinforcement ring or epoxy potting could improve the boundary conditions.

After reaching the buckling load, reference shells rapidly lose load carrying capacity and adopt a post-buckling shape with two rows of uniform half-waves around the circumference as shown in DIC plot in Fig. 5a.

The shells with axial corrugation in Fig. 5b reach a buckling shape with grid-pattern at the average load of 170 N and standard deviation of 12 N. After the buckling, the shells experience uniform deformation at constant load level. As expected, corrugation along the length of the shell does not provide benefits in compression, therefore only the shells with circumferential corrugation are considered for further optimization.

The shells with circumferential corrugation lose load carrying capacity due to out-of-plane displacements around the perimeter of the shell as can be seen in Fig. 5c. Average buckling load for these shells is 2143 N with standard deviation of 126 N. Due to small radius of the corrugation wave, the buckling causes excessive strains in axial direction of the shell which leads to local failure of the material as shown in Fig. 5d. As this process does not happen simultaneously, the shells maintain certain post-buckling load resistance.

Downloaded by TU DELFT on January 7, 2020 | http://arc.aiaa.org | DOI: 10.2514/6.2020-1925

Fig. 5 also reports the buckling load values obtained by the linear eigenvalue analysis and the load-shortening curves of the non-linear FE analysis with imperfection amplitude of 0.05t. It is possible to see that the numerical models predict stiffness and buckling load of the shells accurately enough to be used in further optimization tasks. It is also visible that the buckling load of the corrugated shell is close to the value of linear buckling load, which allows to use this type of analysis to reduce the time necessary for optimization.

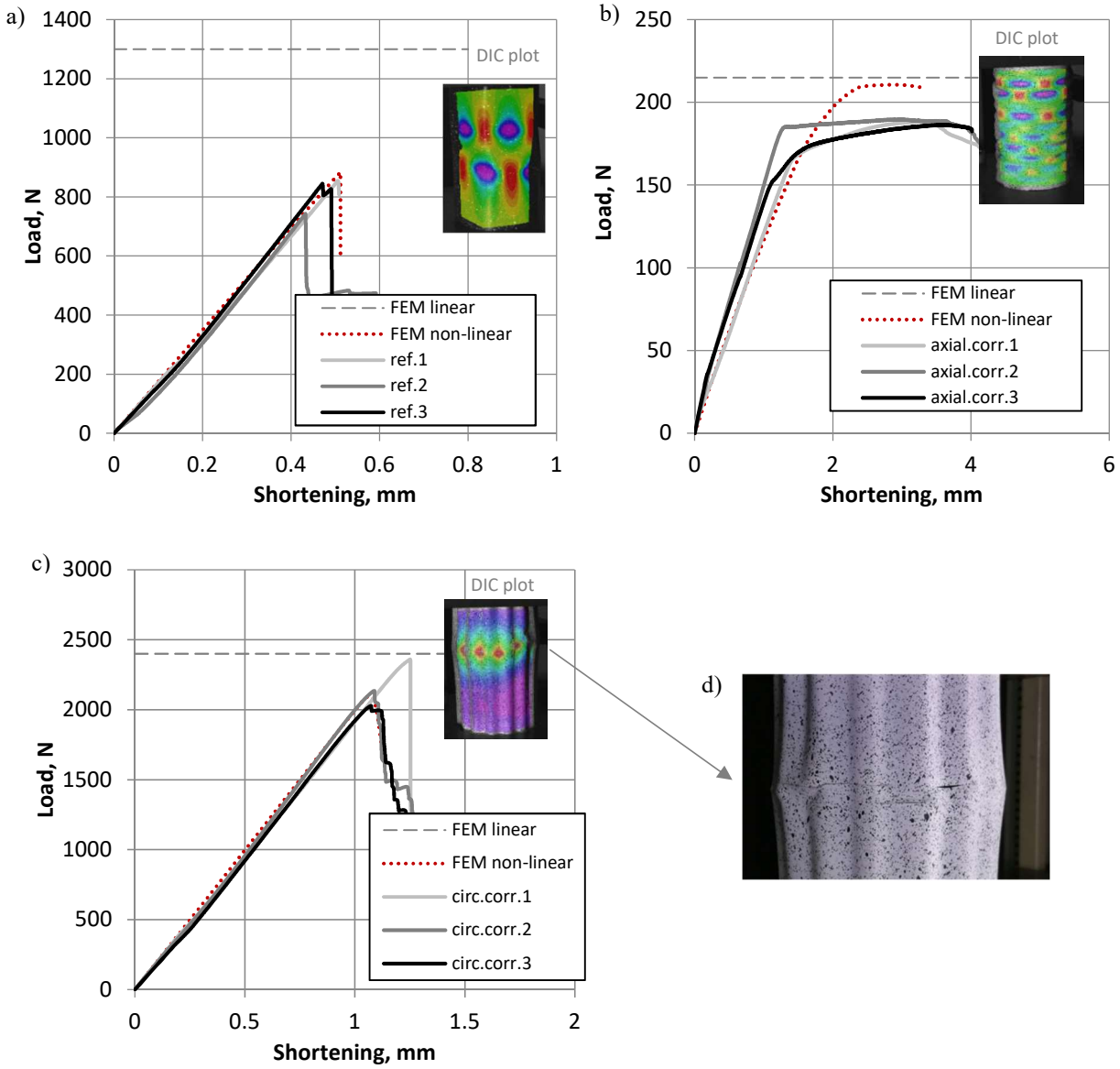

Fig. 5 Load-shortening curves of the tested shells: a) reference shell; b) axially corrugated shell; c) circumferentially corrugated shell; d) material failure for the shell.

VI. Optimization

The shape optimization of the shells is performed to maximize the buckling load while maintaining the same weight. Two cross-section parameters are selected for optimization: the radius/corrugation amplitude ratio and the number of the corrugation waves. The smooth shell with circular surface is set as a reference to evaluate the performance of the corrugated shell. It should be noted that the radius of the shell is increased to 75 mm, maintaining the same height of 170 mm. In this way height/diameter aspect ratio is close to 1, which is commonly used in the studies of shell buckling[19]. The larger radius allows more flexibility, because available printing nozzles have a thickness step of 0.1

Downloaded by TU DELFT on January 7, 2020 | http://arc.aiaa.org | DOI: 10.2514/6.2020-1925

mm. The wall thickness for the reference shell is set to 0.5 mm, that means that the corrugated shell presents smaller thickness, to keep the mass of both shells the same.

The optimization is defined as:

$$\begin{aligned} &maximize: && P_{cr} \\ &subjected\ to: && 0.005 < a_n < 0.05 \\ & && 5 < n < 25 \\ & && m_{ref} = m_{corr} \end{aligned} \tag{2}$$

The optimization is performed employing a parametrical model generated by Python script and executed inside Abaqus. The design of computer experiments (40 combinations) is generated using Latin Hypercube Sampling with random design space filling criteria. Locally weighted smoothing linear regression is used to approximate the responses provided by FE analysis. The maximum value of the function is found using a solver from Matlab Optimization Toolbox.

The approximation surface reported in Fig. 6a shows the relation between the number of the corrugation waves n and the amplitude/radius ratio a_n. The highest linear buckling load of 3650 N is reached by the shell containing 23 corrugation waves and the a_n value of 0.043, that is shown in Fig. 6b. The wall thickness of such a shell is 0.41 mm that provides the same mass as the reference shell with the wall thickness 0.5 mm. Fig. 6c reports the buckling mode of the shell giving lowest response values. The particular example shows that small number of the surface folds forms a hexagonal shell with flat wall sides and weak buckling resistance.

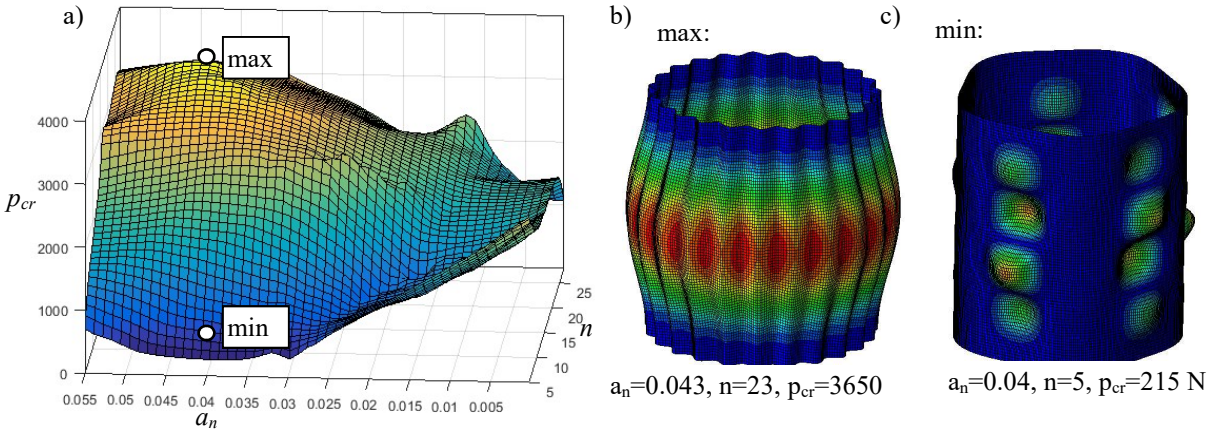

Fig. 6 Optimization results: a) approximation surface of the linear buckling load; b) buckling mode of the shell with the highest eigenvalue; c) buckling mode of the shell with the lowest eigenvalue.

Non-linear analyses are run for the optimized corrugated shell and the reference counterpart to assess the influence of the geometric imperfections. The first eigenmode of the linear buckling analysis is used as source of the initial geometric imperfections in the non-linear analysis. The values of the maximum imperfection amplitude are related to the shell thickness t and have the ratios of 0.02, 0.05 and 0.1. The obtained load-shortening curves are presented in Fig. 7. From these results it is possible to see that both shells have the same stiffness due to equal cross section area, however the buckling load of the corrugated shell is significantly higher and less influenced by geometric imperfections. The analysis also confirms that, while the buckling load of the reference shell is in the range of 74-88% of the linear buckling load, the actual buckling load of the optimized corrugated shell is close to linear buckling load, in the range of 97-99%.

Downloaded by TU DELFT on January 7, 2020 | http://arc.aiaa.org | DOI: 10.2514/6.2020-1925

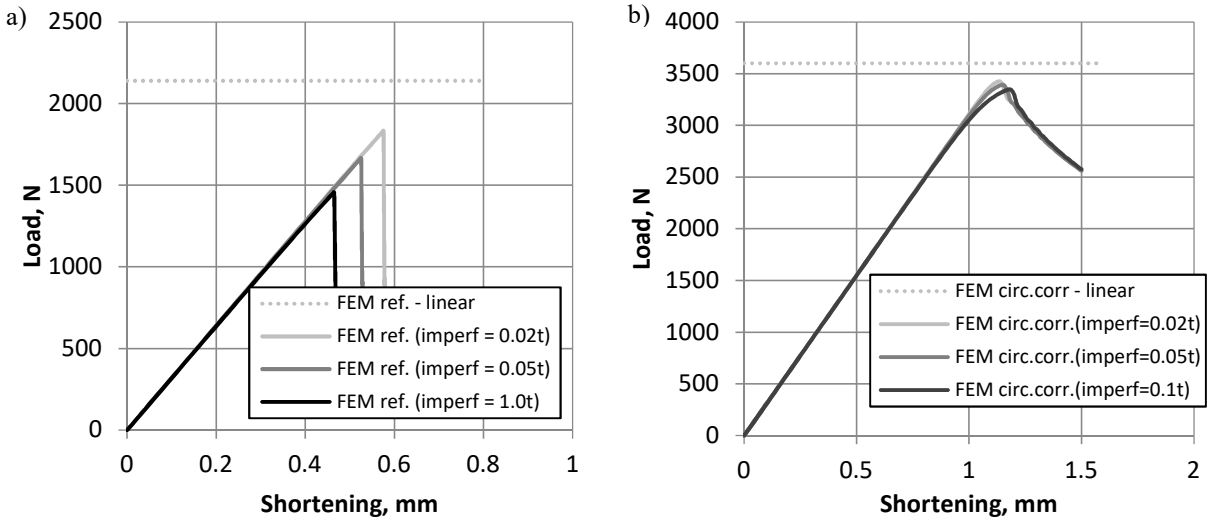

Fig. 7 Linear and non-linear buckling analysis: a) reference shell; b) optimized corrugated shell.

VII. Validation of the Optimized Shells

In order to validate the results obtained by the optimization a new set of three reference and three corrugated shells are manufactured, as shown in Fig. 8. The mass of the shells is kept similar by printing the reference shells with 0.5 mm nozzle and the corrugated shells with 0.4 mm nozzle, so that the weight of the shells is equal to 40 g. The shell prototypes are strengthened with 6 mm thick end-rings made of MDF.

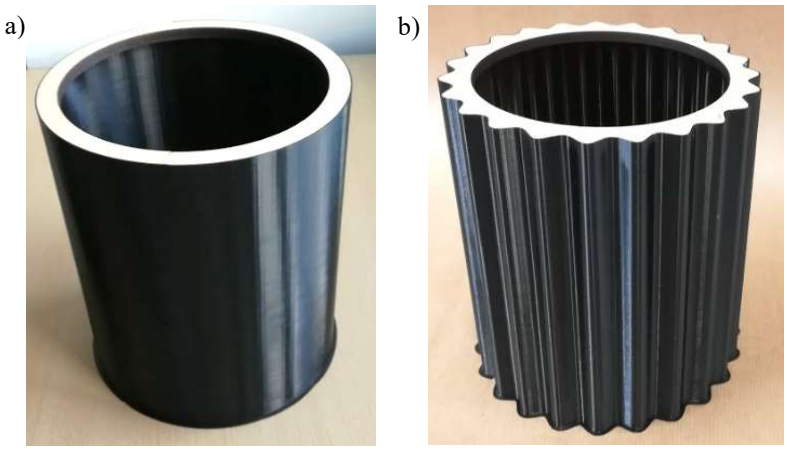

Fig. 8 3D-printed shells: a) reference shell; b) optimized corrugated shell.

The tests are performed using the same test set-up on Zwick Z20 as for the previous smaller diameter shells. Comparison of the experimental and numerical load-shortening curves of the reference shell is given in Fig. 9. Only the numerical curve with the amplitude of geometric imperfection equal to 0.05t is displayed in this plot. Three experimental curves have a close matching stiffness compared to the numerical curve. Observing the buckling load values it is possible to notice that the second reference shell prototype has visibly lower buckling load equal to 1310 N. The lower buckling load of this shell could be explained by the imperfections in the adhesive bond of the reinforcement ring. The buckling load of two other shells are 1684 N and 1576 N, respectively. After the buckling, the shells adopt stable post-buckling mode consisting of two rows of half-waves as shown in Fig. 10a. The color plot

Downloaded by TU DELFT on January 7, 2020 | http://arc.aiaa.org | DOI: 10.2514/6.2020-1925

of the out-of-plane displacements of the buckling shape in Fig. 10b has good agreement with the numerical buckling shape in Fig. 10c. Both experimental and numerical buckling shape contains 7 inner-faced dimples in each row.

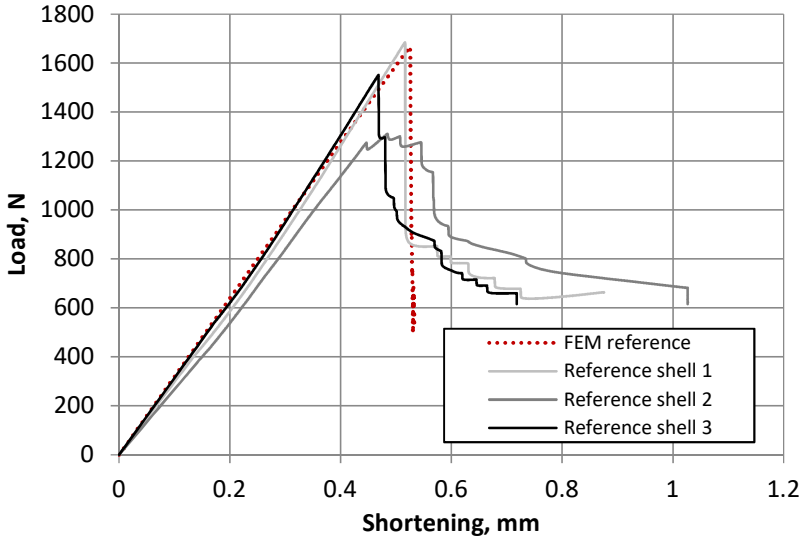

Fig. 9 Experimental and numerical load-shortening curves of the reference shells.

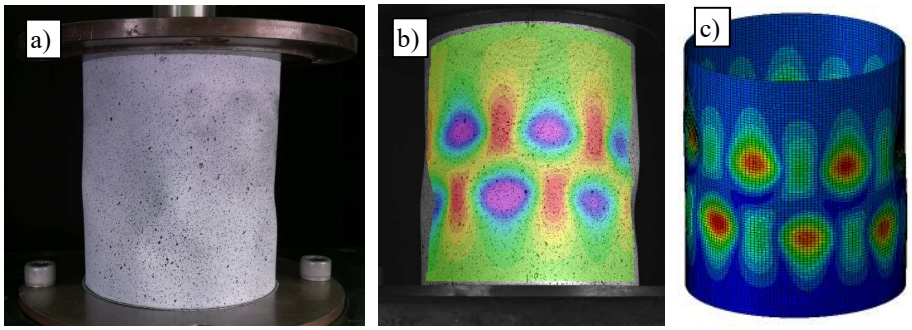

Fig. 10 Reference shell: a) experimental post-buckling shape; b) DIC post- buckling shape; c) FE post-buckling shape.

Comparison of the experimental and numerical load-shortening curves for the optimized corrugated shells are given in Fig. 11. Similar to the reference shells the experimental and numerical curves have a close matching stiffness behavior. The scatter of the buckling loads for these shells is also smaller - in the range of 3190 to 3563 N. The numerically acquired buckling load fits well between the experimental results. By reaching the buckling load, the corrugated shell experiences uniform outward facing out-of-plane displacement as shown in Fig. 12a and Fig. 12b. Similar shape can be observed in the Fig. 12c for the numerical model. Due to small radius of the corrugation, the out-of-plane displacement of the shell causes the material failure.

Downloaded by TU DELFT on January 7, 2020 | http://arc.aiaa.org | DOI: 10.2514/6.2020-1925

Downloaded by TU DELFT on January 7, 2020 | http://arc.aiaa.org | DOI: 10.2514/6.2020-1925

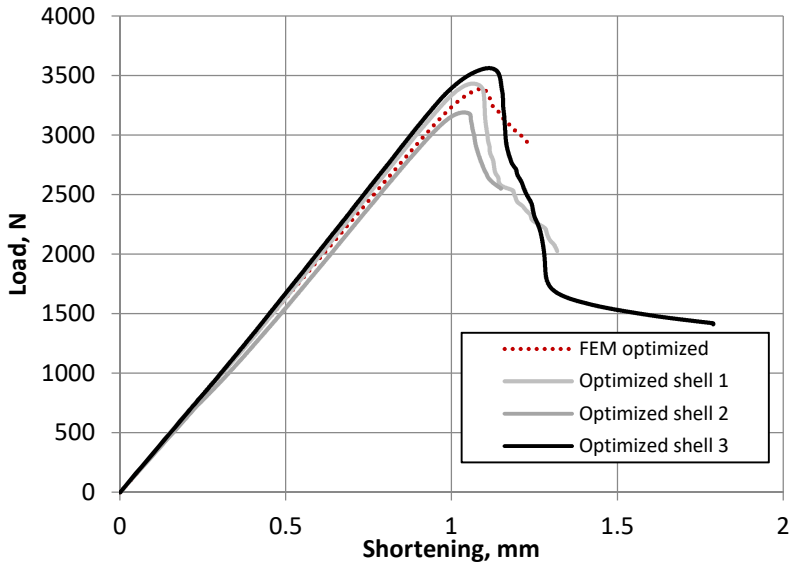

Fig. 11 Experimental and numerical load-shortening curves of the optimized corrugated shells.

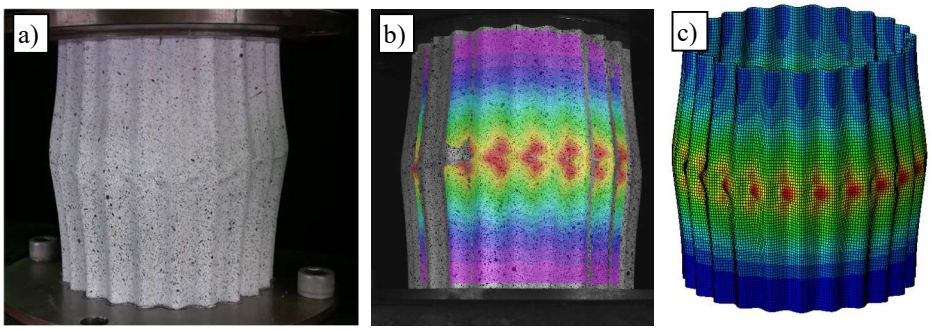

Fig. 12 Optimized corrugated shell: a) post-buckling shape; b) DIC post-buckling shape; c) FE post-buckling shape.

The main results of the tests are summarized in Table 1. The average buckling load of the reference shell is 1523 N with the standard deviation of 157. The numerically predicted buckling load is 10% higher and equal to 1672 N. The average buckling load of the optimized corrugated shells is 3395 N with the standard deviation of 154 N. The numerically predicted buckling load of the optimized shell is closely matching the average test value. The optimized shells have also relatively smaller scatter of the experimental results compared to the reference design. The increase of the buckling load of the optimized corrugated shells compared to the reference shells is 121%.

Table 1. Summary of experimental and numerical results for reference and optimized shells.

Shell type	Buckling load, N	Shortening at the buckling, mm	Buckling load (FE), N	Shortening at the buckling (FE), mm
Reference shell 1	1684	0.51	1672	0.51
Reference shell 2	1310	0.47		
Reference shell 3	1576	0.46		
Optimized shell 1	3433	1.08	3387	1.08
Optimized shell 2	3191	1.03		
Optimized shell 3	3563	1.10		

VIII. Conclusions

In the current study small-scale 3D-printed shells were analyzed numerically and experimentally to evaluate the influence of the corrugation parameters on the buckling load and the sensitivity towards initial geometric imperfections.

A first set of shells were used to gain knowledge on general behavior of 3D-printed shells and validate the numerical model which was further used in optimization of the buckling load. The comparison shows that initial numerical prediction was quite accurate comparing numerical and experimental load-shortening curves.

The parametrical optimization of the shape was used to find a shell with the corrugation along the circumference providing the highest buckling load and, at the same time, maintaining the same mass as the smooth reference shell. The optimization highlights that the buckling load of the corrugated shell can be up to 120% higher comparing to the reference shell. At the same time, the influence of the initial geometric imperfections for the corrugated shells is lower.

The prototypes of the reference and optimized shell with corrugated wall around circumferential direction were manufactured from PLA filament. The experimental axial compression tests confirmed that the mechanical behavior of the shell prototypes matches the numerical predictions, comparing the load-shortening curves and the buckling shapes.

Further research on 3D-printed shells will be conducted to assess the influence of the shell radius, height and thickness on the buckling load of the corrugated shells. Additional experimental tests are also necessary to reduce scatter of the buckling loads for these shells.

Downloaded by TU DELFT on January 7, 2020 | http://arc.aiaa.org | DOI: 10.2514/6.2020-1925

Acknowledgement

The authors would like to thank Dr. David Bushnell for having inspired this research some years ago, before it was possible to manufacture the corrugated shells with 3D-printing technology, and for his contribution in spreading knowledge of shell buckling through his website[20].

References

[1]Praveen A, P., Rajamohan, V., and Mathew, A. T. "Recent Developments in Investigation on Buckling and Post Buckling Responses of Laminated Composite Shells." *Polymer Composites*, Vol. 39, No. 12, 2018, pp. 4231–4242.

[2]Bisagni, C., and Cordisco, P. "An Experimental Investigation into the Buckling and Post-Buckling of CFRP Shells under Combined Axial and Torsion Loading." *Composite Structures*, Vol. 60, No. 4, 2003, pp. 391–402.

[3]Bisagni, C. "Composite Cylindrical Shells under Static and Dynamic Axial Loading: An Experimental Campaign." *Progress in Aerospace Sciences*, Vol. 78, 2015, pp. 107–115.

[4]Labans, E., Bisagni, C., Celebi, M., Tatting, B., Gürdal, Z., Blom-Schieber, A., Rassaian, M., and Wanthal, S. "Bending of Composite Cylindrical Shells with Circular Cutouts: Experimental Validation." *Journal of Aircraft*, Vol. 56, No. 4, 2019, pp. 1534–1550.

[5] Edlund, B. L. O. "Buckling of Metallic Shells: Buckling and Postbuckling Behaviour of Isotropic Shells, Especially Cylinders." *Structural Control and Health Monitoring*, Vol. 14, No. 4, 2007, pp. 693–713.

[6] Abramovich, H., Kalnins, K., and Wieder, A. "Test Results on the Stability and Vibrations of Composite Shells." *Stability and Vibrations of Thin-Walled Composite Structures*, Elsevier, 2017,pp. 619–691.

[7] Rashidi, M. R. W., Frank, G. J., Dohn, T., Seifert, R., Chapkin, W. A., Baur, J. W., and Walgren, P. P. "Biomimicry of the Armadillo Carapace for the Design of Bending Cylinders for Aerospace Applications." *AIAA SciTech Forum*, 2019. Paper number: 1632.

[8] Liu, Y., Zhang, W., Zhang, F., Lan, X., Leng, J., Liu, S., Jia, X., Cotton, C., Sun, B., Gu, B., and Chou, T. W. "Shape Memory Behavior and Recovery Force of 4D Printed Laminated Miura-Origami Structures Subjected to Compressive Loading." *Composites Part B: Engineering*, Vol. 153, No. 15, 2018, pp. 233–242.

[9] Walker, D., Liu, D., and Jennings, A. "Topology Optimization of an Aircraft Wing." *AIAA SciTech Forum 2015*. Paper number: 0976.

[10] Sowiński, K. "Buckling of Shells with Special Shapes with Corrugated Middle Surfaces – FEM Study." *Engineering Structures*, Vol. 179, 2019, pp. 310–320.

[11] Ning, X., and Pellegrino, S. "Imperfection-Insensitive Axially Loaded Thin Cylindrical Shells." *International Journal of Solids and Structures*, Vol. 62, 2015, pp. 39–51.

[12] Ning, X., and Pellegrino, S. "Experiments on Imperfection Insensitive Axially Loaded Cylindrical Shells." *International Journal of Solids and Structures*, No. 115–116, 2017, pp. 73–86.

[13]Wagner, H. N. R., Petersen, E., Khakimova, R., and Hühne, C. "Buckling Analysis of an Imperfection-Insensitive Hybrid Composite Cylinder under Axial Compression – Numerical Simulation, Destructive and Non-Destructive Experimental Testing." *Composite Structures*, Vol. 225, 2019, p. 111152.

[14]White, S. C., and Weaver, P. M. "Towards Imperfection Insensitive Buckling Response of Shell Structures-Shells with Plate-

like Post-Buckled Responses." *The Aeronautical Journal*, Vol. 120, No. 1224, 2016, pp. 233–253.

[15]Labans, E., and Bisagni, C. "Buckling and Free Vibration Study of Variable and Constant-Stiffness Cylindrical Shells." *Composite Structures*, Vol. 210, 2019, pp. 446–457.

[16] Wagner, H. N. R., Köke, H., Dähne, S., Niemann, S., Hühne, C., and Khakimova, R. "Decision Tree-Based Machine Learning to Optimize the Laminate Stacking of Composite Cylinders for Maximum Buckling Load and Minimum Imperfection Sensitivity." *Composite Structures*, Vol. 220, 2019, pp. 45–63.

[17]Technical Data Sheet PLA. Version 3.006, 2017. http://Www.Farnell.Com/Datasheets/2310522.pdf Retrieved 1st November 2019.

[18] Ganev, S., Gendron, G., Cloutier, A., and Beauregard, R. "Mechanical Properties of MDF as a Function of Density and Moisture Content." *Wood and Fiber Science*, Vol. 37, No. 2, 2005, pp. 314–326.

[19] Hilburger, M. W., Nemeth, M. P., and Starnes, J. H. "Shell Buckling Design Criteria Based on Manufacturing Imperfection Signatures." *AIAA Journal*, Vol. 44, No. 3, 2006, pp. 654-663.

[20] Shell buckling Web resource, https://shellbuckling.com Retrieved 1st November 2019.

Downloaded by TU DELFT on January 7, 2020 | http://arc.aiaa.org | DOI: 10.2514/6.2020-1925